Structure and generation mechanism of blue whirls

Shangpeng Li [a,b], Qiang Yao [b,*], Chung K. Law [c,d], Jiankun Zhuo [b],
Huangwei Zhang [a]

[a] *Department of Mechanical Engineering, National University of Singapore, 9 Engineering Drive 1, 117576 Singapore*
[b] *Key laboratory for Thermal Science and Power Engineering of Ministry of Education, Department of Energy and Power
Engineering, Tsinghua University, Beijing 100084, China*
[c] *Department of Mechanical and Aerospace Engineering, Princeton University, Princeton, New Jersey 08544, USA*
[d] *Center for Combustion Energy, Tsinghua University, Beijing 100084, China*

Abstract

Blue whirls are newly discovered blue rotating flames transitioned from fire whirls generated on liquid fuel surfaces. Compared with the traditional fire whirls, blue whirls have a distinct flame structure and are almost soot-free. Studies of the blue whirl are expected to promote the development of clean combustion theory and technology. In this paper, we numerically and theoretically investigate the lifting process of fire whirls and blue whirls, and then discuss their structure and transition mechanisms. In contrast to the explanations in the literature, it is found that blue whirls can be created without the occurrence of bubble-type vortex breakdown in the rotating flow. The blue whirl can be considered as a special form of lifted fire whirl with a considerable liftoff distance and without being blown out. According to the simulation, both blue whirls and fire whirls have the typical triple-flame structure. The unique structure of blue whirls is closely related to the thermal expansion of gas and the restriction of the radial flow by the axis. The theoretical solution of the unified lifting curve for fire whirls and blue whirls is obtained, which is qualitatively in agreement with the numerical result. There are 4 different branches in the lifting curve, two of which are stable, respectively representing fire whirls with small liftoff distances, and blue whirls with larger liftoff distances. The unstable branches between the stable branches lead to non-continuous transitions between fire whirls and blue whirls, as observed in the experiment. The current study explains the existing physical phenomenon and makes valuable predictions that may guide future experiments and simulations.
© 2022 The Combustion Institute. Published by Elsevier Inc. All rights reserved.

Keywords: Blue whirl; Fire whirl; Liftoff; Triple flame; Transition mechanism

1. Introduction

Blue whirl, a rotating flame stabilized over a liquid fuel surface, has been discovered and studied recently [1–10]. In a small-scale experiment, Xiao et al. [1] found that as the circulation of the

---

* Corresponding author.
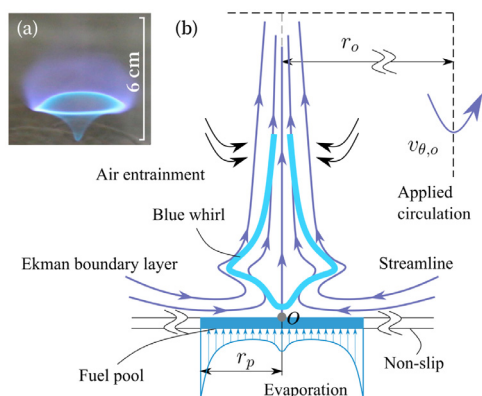*E-mail address:* yaoq@tsinghua.edu.cn (Q. Yao).

Fig. 1. (a) Experimental photograph of a blue whirl [1]; (b) Schematic illustration of a blue whirl. (For interpretation of the references to colour in this figure legend, the reader is referred to the web version of this article.)

rotating flow increases, a sooty and yellow fire whirl can transform into a swirling blue flame, namely blue whirl. As shown in Fig. 1(a), the blue whirl consists of a bright-blue inverted conical flame at the bottom and a faint-violet conical flame above it. Considering that blue whirls are almost soot-free compared to the traditional pool fires and fire whirls, research into the structure and formation mechanism of blue whirls is of interest to the development of clean combustion technology.

Following the pioneering experiment by Xiao et al., several subsequent studies [2–10] have also demonstrated that blue whirls can be generated when small-scale fire whirls on the fuel pool are close to blowout due to excessive circulation. It is shown that in carefully controlled experiments with minimal external perturbations to the flame, the blue whirl can persist for a considerable period of time. According to Coenen et al. [6], as the applied circulation increases, the flame base of the fire whirl detaches from the fuel pool edge and moves toward the center of the flame. During this process, fuel evaporation and flame height decrease due to reduced heat transfer from the flame to the fuel surface. As the circulation increases to a certain extent, the lifted fire whirl transforms into a blue whirl. A preliminary numerical simulation of the blue whirl showed that the blue rim in the middle of the blue whirl has a typical triple-flame structure [9]. Carpio et al. [8] then performed a more detailed numerical simulation of the blue whirl and obtained results that were qualitatively consistent with the experimental results. It is found that the liquid fuel evaporation is primarily driven by the radiative heat transfer from the blue whirl.

Most existing studies [1–10] suggest that blue whirls are generated by bubble-type vortex breakdown in the rotating flow, recognizing that bubble-type vortex breakdown is a typical vortex breakdown phenomenon that occurs in rotating flows,

in which a stagnation point appears along the rotation axis of the flow field and a recirculation zone is formed [11]. It is noted however that while there may indeed be a recirculation zone caused by bubble-type vortex breakdown in the flame region based on the unique shape of the blue whirl, and several numerical simulations have found a recirculation zone in the blue whirl [8,9], it does not necessarily imply that vortex breakdown is necessary for blue whirl generation as there is no solid experimental evidence supporting this conjecture. Furthermore, according to the existing studies [1,6,10], blue whirls have been created only at centimeter scales and cannot be obtained at larger scales yet, it contradicts the fact that vortex breakdown is more likely to occur in large-scale swirling flows.

Based on the above consideration, a thorough investigation of the flame structure and generation mechanism of blue whirls is warranted. Specifically, in our previous work [12], we have analyzed the lifting process of fire whirls under the Boussinesq assumption. A C-shaped r_f-Da lifting curve and the critical blowout limit of fire whirls were derived theoretically by analyzing the structure and propagation of the triple flame at the flame base in the bottom Ekman boundary layer. Since this study is limited to the Boussinesq assumption and restricted to relatively small liftoff distances, no discussion of blue whirls is included.

Consequently, we have now extended the previous study [12] to investigate the liftoff of fire whirls with a broad range of liftoff distances and the generation mechanism of blue whirls. The structure of blue whirls, the unified lifting curves of fire whirls and blue whirls, as well as the transition mechanism of these two flame regimes are identified. The paper is organized as follows. First, Section 2 details the formulation of the problem. Then, the numerical approach is introduced and the results are discussed in Section 3. Based on the obtained numerical results, a theoretical model is developed and analyzed in Section 4.

2. Formulation

The physical problem studied is demonstrated in Fig. 1(b) with the same configuration as in our previous study [12]. Under the influence of a coaxial rotating screen, the pool fire above the liquid fuel surface forms a fire whirl by interacting with the rotating flow. As the circulation of the rotating flow increases to a certain extent, the flame base of the fire whirl detaches from the edge of the fuel pool and the fire whirl is lifted. Usually, the fire whirl blows out directly for considerable liftoff distances. However, by carefully controlling the experimental parameters and minimizing external perturbations, the fire whirl can be transformed into a blue whirl as shown in Fig. 1(a) [1], which has a distinct structure from that of the traditional fire whirl.

A cylindrical coordinate system (r, z, θ) is used with origin at the center of the fuel pool. At a radial position r_o, a coaxial rotating screen with constant rotational velocity, $v_{\theta,o}$, is applied. Assuming that the system is axisymmetric, the nondimensional governing equations read

$$\frac{\partial(\tilde{\rho}\tilde{r}\tilde{v}_r)}{\partial \tilde{r}} + \frac{\partial(\tilde{\rho}\tilde{r}\tilde{v}_z)}{\partial \tilde{z}} = 0,$$

$$\mathcal{L}(\tilde{v}_r) - \tilde{\rho}\frac{\tilde{v}_\theta^2}{\tilde{r}} = -\frac{\partial \tilde{P}}{\partial \tilde{r}} + \tilde{\rho}\left(\nabla^2 \tilde{v}_r - \frac{\tilde{v}_r}{\tilde{r}^2}\right),$$

$$\mathcal{L}(\tilde{v}_\theta) + \tilde{\rho}\frac{\tilde{v}_\theta \tilde{v}_r}{\tilde{r}} = \tilde{\rho}\left(\nabla^2 \tilde{v}_\theta - \frac{\tilde{v}_\theta}{\tilde{r}^2}\right),$$

$$\mathcal{L}(\tilde{v}_z) = -\frac{\partial \tilde{P}}{\partial \tilde{z}} + \tilde{\rho}\nabla^2 \tilde{v}_z - \tilde{\rho}\mathrm{Gr},$$

$$\mathcal{L}\{\tilde{T}, Y_i\} = \tilde{\rho}\mathrm{Pr}^{-1}\nabla^2\{\tilde{T}, Y_i\} + \{+, -\}\,\tilde{\rho}\tilde{\omega}, \quad (1)$$

where tildes denote non-dimensional quantities, and the fuel pool radius, r_p, and the dynamic viscosity, D_u, are used for non-dimensionalization. $\mathcal{L}(\cdot) \equiv \tilde{\rho}(\partial/\partial \tilde{t} + \tilde{v}_r \partial/\partial \tilde{r} + \tilde{v}_z \partial/\partial \tilde{z})(\cdot)$. $\mathrm{Gr} = g r_p^3/D_u^2$ and $\mathrm{Pr} = D_u/D_T$ are the Grashof number and Prandtl number, respectively. $\tilde{T} = (T - T_\infty)/(T - T_{ad})$ is the nondimensional temperature, where T_∞ is the ambient temperature and T_{ad} is the adiabatic flame temperature. A single-step reaction is considered for simplicity and $\tilde{\omega} = \tilde{\rho}\,\mathrm{Da}\,Y_F Y_O \exp(-\mathrm{Ze}\,(1 - \tilde{T})/(1 - \alpha\,(1 - \tilde{T})))$, where F and O represent fuel and oxygen, respectively. α, Da and Ze are respectively the thermal expansion factor, the Damköhler number and the Zel'dovich number. Unity Lewis number is assumed for all species.

The boundary conditions can be found in Ref. [12]. As shown in Fig. 1(b), the main boundary conditions consist of the rotating screen boundary condition at radius r_o, $v_{\theta,o} r_o/D_u \equiv \mathrm{Ek}$, and the fuel surface evaporation boundary condition. For simplicity, thermal radiation from the flame to the fuel surface, and thermal conduction in the liquid phase are not directly calculated. Instead, the evaporation intensity of the liquid fuel surface is characterized by the Spalding numbers relevant to the local energy absorption at the fuel surface. Considering that the heat transfer from the flame to the fuel surface is related to the radial position of the lifted flame base, $\tilde{r}_f$ [12], two different Spalding numbers, B_v and B_q, are used to characterize the evaporation intensity of the liquid fuel for two different regions with $\tilde{r} > \tilde{r}_f$ and $\tilde{r} < \tilde{r}_f$, respectively. Specifically, the evaporation boundary condition of the fuel surface is given as: $\tilde{v}_z = -\mathrm{Pr}^{-1}B_v\,(\partial Y_F/Y_{F,s})/\partial \tilde{z}$ and $Y_F = B_v/(1 + B_v)$ for $\tilde{r} > \tilde{r}_f$; while $\tilde{v}_z = \mathrm{Pr}^{-1}B_q \partial \tilde{T}/\partial \tilde{z}$ and $Y_F = 1$ for $\tilde{r} \leq \tilde{r}_f$. The subscript s represents the fuel surface.

3. Numerical approach & result discussion

The governing Eq. (1) subject to the above mentioned boundary conditions is solved numerically until reaching the steady state. The two-dimensional axisymmetric simulation region has $\tilde{r} \in [0, 3]$ and $\tilde{z} \in [0, 30]$. Locally refined grids are achieved in the triple-flame region at the flame base with a minimum grid size of $\Delta \tilde{r} = \Delta \tilde{z} = 2 \times 10^{-5}$. A sensitivity analysis was performed before determining the geometry, mesh, and step size. Referring to our previous study [12], the following parameter values are used by default in simulations if not specified otherwise: $\alpha = 0.7$, Ze $= 7.0$, Pr $= 1$, $B_q = 10$, $B_v = 2$, Gr $= 4 \times 10^4$, and Ek $= 800$.

The numerical approach is similar to that of Ref. [12]. For a given radial liftoff position of the flame, $\tilde{r}_f$, the solutions to the eigenvalue, Da, of the governing Eq. (1) are iteratively found in the simulation. This approach allows grid refinement of the triple-flame region before computation. Moreover, a complete set of solutions can be obtained for specific flow parameters and boundary conditions, including both stable and unstable solutions. Upon obtaining the eigenvalue Da for a given $\tilde{r}_f$, the flame is slightly perturbed and its subsequent behavior indicates the stability of the solution.

It is noted that the liftoff process of fire whirls is hysteretic and may involve several different liftoff positions for a particular Da. Compared with our previous study, the current simulation considers the effect of thermal expansion and broadens the range of the calculated liftoff distances. Consequently, all branches of the lifting curve, including the blue whirl branch, can therefore be found, resulting in a complete lifting curve for both fire whirls and blue whirls.

3.1. Flame lifting curve & blue whirl formation

Fig. 2 (a) presents the numerical solution of fire whirls at different liftoff distances. In the bottom Ekman boundary layer of fire whirls, as the liftoff distance increases, the flame base of fire whirls moves closer to the axis and then $\tilde{r}_f$ decreases. During this process, the fuel evaporation and the flame height decrease due to reduced heat transfer from the flame to the fuel surface. When the liftoff distance decreases to a certain point, say $\tilde{r}_f = 0.1$, the flame structure approximates that of the experimentally observed blue whirl with an open bottom tip [6].

It is seen from Fig. 2(a) that as $\tilde{r}_f$ decreases, the triple flame at the flame base increases in size and is distorted in shape, and the flame profile gradually transforms from being outwardly convex to concave. As a result, blue whirls have a distinct structure that differs from the traditional fire whirls. The simulation results indicate that variation of the triple flame structure is primarily due to thermal expansion of the flow passing through the triple flame, as well as the restricted radial flow near the axis with small $\tilde{r}$ since $\tilde{v}_r = 0$ at $\tilde{r} = 0$.
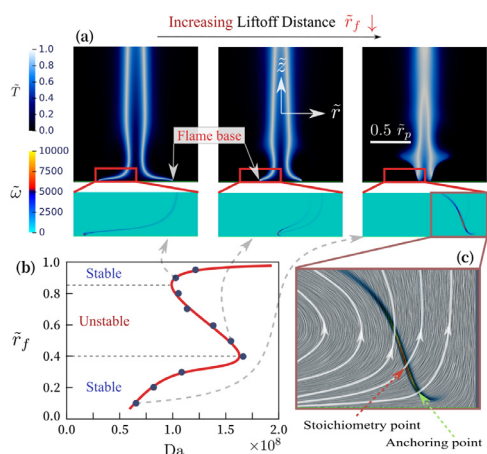
Fig. 2. (a) Numerical results of $\tilde{T}$ and $\tilde{\omega}$ of a lifted fire whirl with increasing liftoff distance; (b) Numerical results of the $\tilde{r}_f$-Da lifting curve for lifted fire whirls and blue whirls; (c) Streamlines around the triple flame at the base of the lifted fire whirl with $\tilde{r}_f = 0.1$. (For interpretation of the references to colour in this figure legend, the reader is referred to the web version of this article.)

The fuel and air are well mixed before combustion due to the large liftoff distances of blue whirls. Consequently, as shown in Fig. 2(a), the trailing diffusion flame of the triple flame almost disappears, and the flame mainly consists of two partially premixed flames, with fuel-lean and -rich compositions. Therefore, blue whirls produce less soot than the traditional fire whirls, and their flames are blue instead of bright yellow, which agrees with the experiments [1,6,10].

The calculated relation between $\tilde{r}_f$ and Da for the liftoff process is given in Fig. 2(b). It is seen that the $\tilde{r}_f$-Da lifting curve has 3 different branches within the calculated range of the liftoff distances, resulting in an S-shaped curve. In our previous study [12], because of limited liftoff distances, only two branches of the S-shaped curve are obtained, showing a C-shaped curve. Additionally, Fig. 2(b) shows that the first and third branches of the $\tilde{r}_f$-Da curve are stable, while the second branch in between is unstable.

No rigorous definition of blue whirls has yet been provided in the literature. Referring to the $\tilde{r}_f$-Da lifting curve shown in Fig. 2(b), we attempt to provide a straightforward and reasonably rigorous definition that distinguishes blue whirls from the traditional fire whirls. First, the first stable branch with a relatively small liftoff distance can be deemed a fire whirl. In contrast, the other stable branch (i.e., the third branch) can be categorized as a blue whirl. Then, the unstable branch between the two stable branches is physically difficult to sustain, representing the transition state between fire whirls and blue whirls. It is easy to determine the flame

regime in the experiment with the current classification because the unstable branch causes a non-smooth transition between the two flame regimes, which is observed in the experiments [1,6].

According to Fig. 2(b), shifting from the firewhirl to blue-whirl regime requires a gradual decrease in Da, while the opposite is true when shifting from the blue-whirl to fire-whirl regime. The transition from the fire-whirl regime to the blue-whirl regime requires careful manipulation, e.g., slow adjustment of flow parameters such as circulation intensity, and minimization of external perturbations to avoid blowout of the flame. The blue whirl is located in a considerably broad stable region after it is established. Therefore, it can remain relatively stable despite external perturbations. Under certain conditions, some branches of the lifting curve may merge or disappear. For example, the vanishing of the second branch will lead to the merging of the two stable branches, in which there is no transition state between these two flame regimes, thus making it unnecessary to distinguish them.

3.2. Structure of blue whirls

As observed in the experiment, blue whirls can either have an open or closed bottom tip [1]. A tip-closed blue whirl can be obtained if the liftoff distance is further increased, as shown in Fig. 3(a). We found that the tip-closed blue whirl can only be obtained when the Spalding number of the fuel surface, B_v, is close to 1, and as such the mixture composition approaches stoichiometry near the surface. Under this situation, the bottom tip of blue whirls near the fuel surface keeps burning without being extinguished.
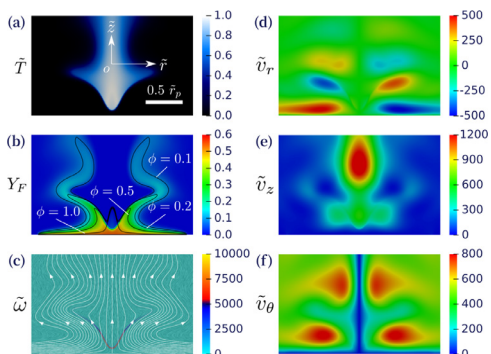

Fig. 3. Numerical results of blue whirls ($B_v = 1.2$, the nondimensional distance between the blue-whirl tip and the fuel surface is 0.08): (a) Temperature, $\tilde{T}$; (b) Fuel concentration, Y_F, and equivalence ratio, ϕ; (c) Reaction rate, $\tilde{\omega}$, and streamline; (d-f) Three components of the velocity. (For interpretation of the references to colour in this figure legend, the reader is referred to the web version of this article.)

The numerical result of the blue whirl structure shown in Fig. 3(a) generally matches the existing experimental results (e.g., as shown in Fig. 1(a)). The distributions of the fuel concentration and the equivalence ratio, ϕ, in the blue whirl are given in Fig. 3(b). It is shown that the entire blue whirl can be viewed as a triple flame, except that its trailing diffusion flame is relatively weak and almost vanishing. In the given conditions, the triple flame's leading tip does not lie on the blue ring of the blue whirl. In addition to the mixture composition near the liquid surface, the leading tip position may also be affected by the reaction mechanism used in the simulation.

According to the streamlines given in Fig. 3(c) and the contours of the three velocity components given in Figs. 3(d-f), there is no stagnation point or recirculation zone in the flow field of the blue whirl, indicating that no bubble-type vortex breakdown occurs as previously assumed [1,10]. Consequently, our study implies that vortex breakdown is unnecessary for the generation of blue whirls. In fact, there is no conclusive experimental evidence of the existence of a stagnation point or a recirculation zone in the flow field of blue whirls. In addition, vortex breakdown is more likely to occur in large-scale swirls; however, the blue whirl has only been created in centimeter-scale experiments so far and cannot be obtained at larger scales [1,6,10]. Furthermore, while several numerical simulations have found a recirculation zone in the blue whirl [8,9], the direct relation between vortex breakdown and blue whirl generation has not been established yet. Finally, the blue whirl generated in the experiment [1] is relatively stable with a smooth flame surface (see Fig. 1(a)), while vortex breakdown usually causes local perturbation or even turbulence. Therefore, it is possible that the observed blue whirl did not exhibit vortex breakdown.

According to Figs. 2(a,c) and Fig. 3(c), the distinct difference between the flame shape of blue whirls and fire whirls is due to the fact that, as the liftoff distance of fire whirls increases to a certain extent, the flow passing through the triple flame at the flame base is significantly deflected by thermal expansion combined with the constraints imposed by the rotating axis. The triple flame is greatly distorted with the flow for large liftoff distances, resulting in a unique structure of blue whirls compared with fire whirls.

4. Theoretical analysis

We have previously analyzed the fire whirl lifting process under the Boussinesq assumption [12]. With this assumption, only the buoyancy effect is considered, while the perturbation of the flow by the thermal expansion of gas is neglected. According to our simulations, a blue whirl is transi-

tioned from a fire whirl at relatively large liftoff distances, and it is severely affected by thermal expansion. Therefore, to analyze the structure and generation mechanism of blue whirls, we shall relax the Boussinesq assumption and consider the thermal expansion effect, extending the previous studies to a broader range of liftoff distances.

4.1. Fire whirl liftoff under Boussinesq assumption

Here we start with a brief overview of the previous theoretical model on the liftoff of fire whirls under the Boussinesq assumption [12]. By analyzing the stabilization of the triple flame at the flame base in the bottom Ekman boundary layer, the liftoff position of the fire whirl is determined by the equilibrium equation of the triple flame propagation speed, $\tilde{S}_L$, and the local flow velocity, $\tilde{v}_f$, as $\tilde{v}_f = \tilde{S}_L$, and then we obtain

$$n_v \mathrm{Pr}^{-\frac{1}{3}} \mathrm{Ek} \frac{1}{F(\tilde{r}_f)\tilde{r}_f} = \mathrm{Re}_p - n_s \mathrm{Pr}^{\frac{1}{3}} \mathrm{Ek}^{\frac{1}{2}} \frac{F(\tilde{r}_f)}{\tilde{r}_f}, \quad (2)$$

where $\mathrm{Re}_p = S_L^S r_p / D_u$ and S_L^S is the stoichiometric planar flame speed. n_v and n_s are two constants given as $n_v = (6\sigma^2)^{1/3}\xi_{St}$ and $n_s = 2^{1/2}(\sigma/6)^{1/3}$ $\mathrm{Ze}Y_{F,s}|Z'(\xi_{St})|$, respectively ($\sigma = 0.5433$). Based on Refs. [12,13], the analytic solution of the mixture fraction, Z, can be derived subject to the local similarity variable, $\xi = (\sigma \mathrm{Pr}/6)^{1/3}\mathrm{Ek}^{1/2}\tilde{z}F(\tilde{r})/\tilde{r}$ and $F(\tilde{r}) = (\tilde{r}^{-3/2} - 1)^{-1/3}$. The subscript *St* represents the stoichiometric composition.

4.2. Extension to a broader range of liftoff distances

In Ref. [12], the concentrated vortex above the bottom Ekman boundary layer is presumed to be a free vortex, i.e., the rotational velocity of the main flow is $\tilde{v}_{\theta,m} \propto 1/\tilde{r}$. Experimental and simulation results indicate that the concentrated vortex in the bulk flame region of fire whirls can be approximated as a Burgers vortex. The Burgers vortex consists of an inner solid rotating vortex and an outer free vortex. Its distribution is expressed as $\tilde{v}_{\theta,m} = \mathrm{Ek}(1 - \exp(-(\gamma\tilde{r}/\tilde{r}_c)^2))/\tilde{r}$, where $\tilde{r}_c$ is the vortex core radius and $\gamma = 1.12$. Consequently, the theoretical analysis in Ref. [12] is only applicable to the situation with $\tilde{r}_f > \tilde{r}_c$, i.e., when the liftoff distance of fire whirls is relatively small.

According to our simulation results, when Gr is considerably large (e.g., $\mathrm{Gr} = 64 \times 10^4$), the vortex core radius $\tilde{r}_c$ is much smaller than the fuel pool radius $\tilde{r}_p$. In this case, the main rotational velocity profile of fire whirls agrees well with that of the Burgers vortex. However, when Gr is relatively small (e.g., $\mathrm{Gr} = 1 \times 10^4$), $\tilde{r}_c$ is even larger than $\tilde{r}_p$. Thus, the rotating flow above the fuel pool can no longer be regarded as a free vortex. Additionally, owing to the nature of axisymmetric rotating flows,

$\tilde{v}_\theta$ always reduces to 0 at the axis, which also limits the applicability of the previous theory.

A straightforward attempt to overcome the limitation of the original theoretical model is to replace the global Ekman number, Ek, with the local Ekman number, $Ek_e(r) \equiv v_\theta(r)r/D_u$, in the derivation. Ek_e is equal to Ek for the free vortex. For the Burgers vortex, Ek_e is approximately constant and equals to Ek at $\tilde{r} > \tilde{r}_c$. While for regions with $\tilde{r} < \tilde{r}_c$, Ek_e decreases continuously as $\tilde{r}$ decreases, and reduces to 0 at $\tilde{r} = 0$. By incorporating Ek_e into the model, the singularity of theoretical solutions of physical quantities at the axis is also eliminated. For example, as $\tilde{r} \to 0$, the current solution of $\tilde{v}_{r,f}$ approaches a finite value rather than infinity as it does in the previous model. Though the approach is not mathematically rigorous, it provides a simple way for extending the existing theory to all radial liftoff positions of fire whirls. In fact, the boundary layer assumption fails as $\tilde{r} \to 0$, and as such the complete Navier-Stokes equation should be considered instead, although it is challenging to obtain a complete global solution for this problem by rigorous derivations. Following the derivation of our previous work and introducing $Ek_e(\tilde{r})$ into the model, the local fuel evaporation rate, $\tilde{v}_{z,0}$, and the flame position, $\tilde{z}_{St}$, at the bottom Ekman boundary layer of fire whirls can be obtained. It is noted that the current method can be applied to general forms of concentrated vortex that do not satisfy the Burgers vortex distribution.

4.3. Considering axial velocity & thermal expansion

As the liftoff distance of a fire whirl increases and the flame base gets closer to the axis, the axial velocity at the triple-flame region increases while the radial velocity decreases. Consequently, the axial velocity for relatively large liftoff distances shall no longer be neglected. Based on the derivation in Ref. [12] and omitting the relatively small term, the axial velocity in the bottom boundary layer of fire whirls is

$$\tilde{v}_z \approx \frac{\sigma}{2} Ek_e(\tilde{r})^{\frac{3}{2}} \frac{z^2}{\tilde{r}^3}. \tag{3}$$

With a large Zel'dovich number and a small traversal velocity gradient (TVG) in the boundary layer, the effect of TVG on the structure and apparent propagation speed of the triple flame is negligible [12]. By ignoring the TVG effect, the leading tip of the triple flame is located at the stoichiometric position, where the axial velocity of the flow is

$$\tilde{v}_{z,f} = \frac{\sigma}{2} \xi_{St}^2 Ek_e(\tilde{r})^{\frac{1}{2}} \frac{1}{\tilde{r} F(\tilde{r})^2}. \tag{4}$$

As a comparison, the radial velocity at the same position is

$$\tilde{v}_{r,f} = \sigma \xi_{St} Ek_e(\tilde{r}) \frac{1}{\tilde{r} F(\tilde{r})}. \tag{5}$$

According to Eqs. (4) and (5), $\tilde{v}_{r,f}$ is much larger than $\tilde{v}_{z,f}$ in most of the radial positions along the stoichiometric line. As the flame base is lifted close to the axis (e.g., $\tilde{r}_f \lesssim 0.1$), $\tilde{v}_{z,f}$ increases rapidly, whereas $\tilde{v}_{r,f}$ decreases quickly to 0. Therefore, $\tilde{v}_{z,f}$ needs to be considered in the current study for a broad range of liftoff distances. This is different from our previous analysis, in which $\tilde{v}_{z,f}$ can be safely ignored since $\tilde{r}_f > 0.5$ was studied.

As a result of the high flame temperature in fire whirls and blue whirls [2], thermal expansion of gas is generally not negligible. Based on the asymptotic analysis of the triple flame propagation in uniform flows by Ghosal et al. [14] and the derivation given in Ref. [12], the dynamic equilibrium of the triple flame of lifted fire whirls including the thermal expansion effect and the axial velocity is written as $\tilde{v}_{f,\alpha} = \tilde{S}_L$, which can be expanded to

$$\tilde{v}_{f,\alpha} \equiv \sqrt{\left(\frac{\tilde{v}_{r,f}}{J_l(\alpha)}\right)^2 + \left(\frac{\tilde{v}_{z,f}}{J_0(\alpha)}\right)^2} = \tilde{S}_L, \tag{6}$$

where $J_l(\alpha) = 1 + l\alpha$ quantifies the effect of the thermal expansion on the apparent propagation speed of the triple flame, with $l = 1$ in the case of uniform flows in the absence of nearby surfaces [14]. Due to the complexity of the current problem, it is challenging to obtain a theoretical expression of l. Considering that as the triple flame approaches the axis and $\tilde{r}_f$ decreases, the thermal expansion effect coupled with the restriction of the radial flow by the axis results in a greater slowdown of $\tilde{v}_r$, therefore $J_l(\alpha)$ is expected to increase with decreasing $\tilde{r}_f$. For this reason, we simply let $l = 3.5 - 2.0 \tilde{r}_f$ in combination with the numerical results. Since there are no direct constraints on the axial flow by the axis, $l = 1$ and as such $J_0(\alpha) = 1 + \alpha$, which does not vary with $\tilde{r}_f$, is applied to the term containing $\tilde{v}_{z,f}$ in Eq. (6).

4.4. Solutions to liftoff of fire whirls & blue whirls

Substituting the expressions of $\tilde{v}_{r,f}$, $\tilde{v}_{z,f}$ and $\tilde{S}_L$ into Eq. (6) yields

$$\sqrt{\left(\frac{1}{J_l(\alpha)} \frac{n_{v,r} Ek_e(\tilde{r}_f)}{\tilde{r}_f F(\tilde{r}_f)}\right)^2 + \left(\frac{1}{J_0(\alpha)} \frac{n_{v,z} Ek_e(\tilde{r}_f)^{1/2}}{\tilde{r}_f F(\tilde{r}_f)^2}\right)^2}$$
$$= Re_p - \frac{1}{(1-\alpha)J_l(\alpha)^2} n_s Ek_e^{1/2} \frac{F(\tilde{r}_f)}{\tilde{r}_f}, \tag{7}$$

where $n_{v,r} = \sigma \xi_{St}$, $n_{v,z} = (\sigma/2)\xi_{St}^2$, $n_s = \sqrt{2} Ze$ $Y_{F,s} Z'(\xi_{St})$. Equation (7) is an algebraic equation for the radial liftoff position, $\tilde{r}_f$. As such, the liftoff distance for given conditions can be obtained with a simple calculation of Eq. (7).

Based on the left and right terms of Eq. (7), Figs. 4(a-d) show the distributions of the propagation speed, $\tilde{S}_L$, and the flow velocity, $\tilde{V}_{f,\alpha}$, along the
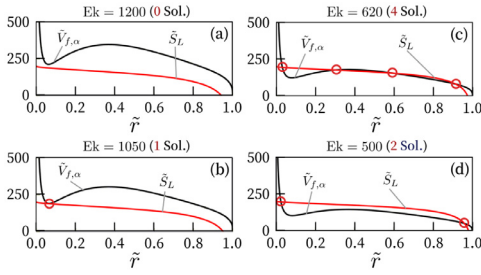
Fig. 4. Theoretical solutions of the triple flame propagation speed, $\tilde{S}_L$, and the flow velocity, $\tilde{v}_{f,\alpha}$, along the stoichiometric line for various Ek ($Re_p = 200$).
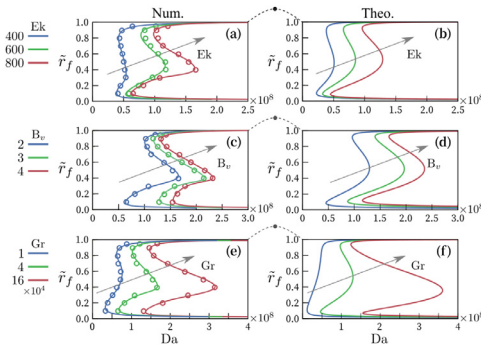

Fig. 5. Comparison of theoretical and numerical results of $\tilde{r}_f$-Da curves under varied Ek, B_v, and Gr. a) $B_v = 2$ and Gr $= 4 \times 10^4$; b) Gr $= 4 \times 10^4$ and Ek $= 800$; c) $B_v = 2$ and Ek $= 800$.

stoichiometric line in the boundary layer for various Ekman numbers. Each intersection point of the two curves in the figure represents a solution to Eq. (7). Fig. 4(a) shows that Eq. (7) has no solutions for too large values of Ek, at which the fire whirl blowouts. As Ek decreases, one solution appears, which is close to the axis (see Fig. 4(b)). It corresponds to the solution of blue whirls. If Ek continues to decrease, the number of solutions gradually increases to a maximum of 4 (see Fig. 4(c)), and then decreases again. When Ek decreases to a certain extent, only two solutions exist, with one close to the edge of the fuel pool and the other close to the axis (see Fig. 4(d)). As Ek further decreases, these two solutions respectively move toward the axis and the fuel pool edge.

Theoretical results of the lifting curves of fire whirls are obtained by plotting all the solutions as shown in Figs. 4(a-d) on the $\tilde{r}_f$-Da coordinate system. As illustrated in Figs. 5(a-f), the theoretical solution of the lifting curves agrees qualitatively with the numerical result for a wide range of parameters, successfully providing each branch of the curve. The theory correctly predicts the trend of the influence of various parameters on the lifting pro-

cess. It is seen that as Ek, B_v or Gr increases, the $\tilde{r}_f$-Da curve shifts to the right, which means a larger Da is required for the same liftoff distance, and the flame is more likely to liftoff and blowout. A larger Ek represents a stronger rotational flow while a larger Gr represents a more significant buoyancy effect, which can both intensify the flow in the bottom Ekman boundary layer. On the other hand, the increase of B_v causes the stoichiometric line in the boundary layer to shift outward, thereby increasing the local flow velocity subjected to the triple flame. Since the effect of the cold surface on the triple flame is not considered in our model, the required Da for flame stabilization is underestimated for relatively small B_v, in which the triple flame is too close to the cold surface and the heat loss increases.

4.5. Unified lifting curve & transition mechanism

Based on the above analysis, blue whirls are generated from significantly lifted fire whirls. Both lifted fire whirls and blue whirls have the structure of a triple flame, but the size, position and shape of the triple flame vary with different liftoff distances. Consequently, the blue whirl can be considered as a special form of the fire whirl. To better understand the transition mechanism between fire whirls and blue whirls, it is necessary to consider the lifting curves of these two flame regimes in a unified approach.

In normal circumstances, the size of the triple flame at the flame base of a lifted diffusion flame is relatively small, for which the distance between the flame base and the location where the fuel and air start to mix can be taken directly as the liftoff distance. However, when the size of the triple flame is considerably large, as with the blue whirl studied in this paper, the position of each point on the triple-flame profile differs significantly. Here we propose a general definition of the liftoff distance, L_f: the distance between the anchoring point of the lifted flame base and the position where the initial fuel/oxidizer mixing starts (e.g., fuel pool edge for the current study). As indicated in Fig. 2(c), the anchoring point is where the flame surface is perpendicular to the local flow velocity, which plays an essential role in the propagation and stabilization of lifted diffusion flames.

For fire whirls with small liftoff distances, the anchoring point is located close to the triple flame's stoichiometric position. As shown in Fig. 2(a), when the liftoff distance of the fire whirl increases or even a blue whirl forms, the shape of the triple flame is significantly twisted, and the anchoring point shifts downward towards the bottom of the blue whirl (see Fig. 2(c)). As illustrated in Fig. 3(a), the anchoring point of the triple flame ultimately reaches the bottom tip position of the blue whirl. In order to simplify the process and make it easier to observe the overall lifting curve, we let $L_f =$
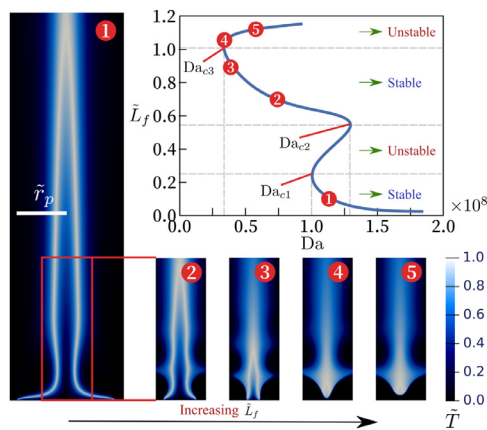
Fig. 6. Numerical results of the unified lifting curve for fire whirls and blue whirls ($B_v = 1.2$). (For interpretation of the references to colour in this figure legend, the reader is referred to the web version of this article.)
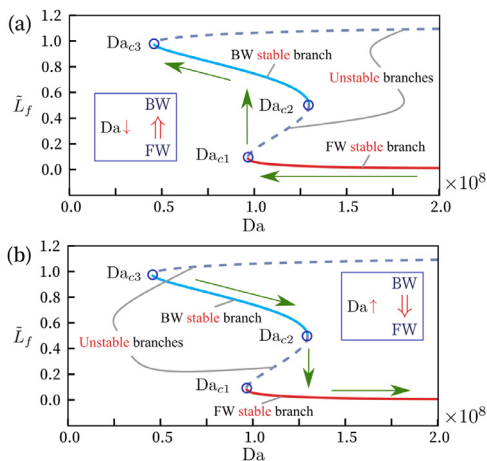

Fig. 7. Transition mechanism of lifted fire whirls (FWs) and blue whirls (BWs): (a) Transition from fire whirls to blue whirls; (b) Transition from blue whirls to fire whirls. (For interpretation of the references to colour in this figure legend, the reader is referred to the web version of this article.)

$(r_p - r_f) + z_f$ for lifted fire whirls or blue whirls with an open tip, while letting $L_f = r_p + z_f$ for blue whirls with a closed tip.

Fig. 6 shows the numerical results of the unified $\tilde{L}_f$-Da lifting curve of fire whirls and blue whirls. It is seen that the lifting curve has 4 different branches, two of which are stable while the other two are unstable. There are 3 critical points between these branches, namely ($\text{Da}_{c1}, \tilde{L}_{f,c1}$), ($\text{Da}_{c2}, \tilde{L}_{f,c2}$) and ($\text{Da}_{c3}, \tilde{L}_{f,c3}$), which respectively correspond to the transition from fire whirls to blue whirls, the transition from blue whirls to fire whirls, and the blowout limit of blue whirls. Different branches of the unified lifting curve may merge in some instances, which would allow the transition process between blue whirls and fire whirls to be continuous.

According to Fig. 6, the slightly lifted fire whirl and the blue whirl with open tip are in the stable branch. It is found that the blue whirl tends to become unstable when the bottom tip is closed, which can be due to that the topology of the triple flame on blue whirls is essentially changed after the tip closure, causing perturbations to the flame. Additionally, considering that fire whirls and blue whirls are in dynamic stability in actual experiments [1,6], blue whirls may be in a dynamic stable state after tip closure and harder to achieve static stability. The current study only examines the static stability of the physical processes. In dynamically stable lifting processes, the $\tilde{L}_f$-Da lifting curves will change accordingly.

Based on the relation between the liftoff distance, $\tilde{L}_f$, and $\tilde{r}_f$ given above, the theoretical solution of $\tilde{L}_f$ can be derived from Eq. (7). The analytical result of the $\tilde{L}_f$-Da lifting curve is given in Fig. 7, in which the transition mechanism of

lifted fire whirls and blue whirls is also indicated. It is seen that the hysteretic lifting process leads to irreversible transitions between these two flame regimes. As shown in Fig. 7(a), Da needs to be gradually reduced in order to transform fire whirls into blue whirls, provided all other parameters are fixed. When Da decreases to less than Da_{c1}, $\tilde{L}_f$ suddenly increases, and the flame regime jumps from the fire-whirl branch to the blue-whirl branch. As illustrated in Fig. 7(b), the transition from fire whirls to blue whirls requires a gradual increase in Da. As Da becomes larger than Da_{c2}, $\tilde{L}_f$ suddenly decreases, and the flame regime jumps from the blue-whirl branch to the fire-whirl branch. It is noted that Fig. 7 only shows the lifting curve for a specific set of parameters. By changing parameters such as Ek, Gr, and B_v, the 4 branches will be adjusted accordingly. It is possible for different branches to merge and for critical points to disappear under certain circumstances.

The theoretical analysis in this paper not only explains the existing experimental phenomenon but also provides guidance for future experimental designs. For example, according to Fig. 7(a), if $\text{Da}_{c1} < \text{Da}_{c3}$, the transition from a fire whirl to a blue whirl becomes difficult to control, and the fire whirl tends to blowout directly. While for $\text{Da}_{c2} < \text{Da}_{c3}$, the blue-whirl branch disappears, which means no blue whirl can be generated under this condition. Our analysis shows that to obtain stable blue whirls, it is essential to choose appropriate parameters to widen the blue-whirl branch in the lifting curve.

5. Conclusions

The liftoff of fire whirls and blue whirls, as well as the structure and transition of these two types of flames, are numerically and theoretically investigated. It is found that blue whirls can be generated without the occurrence of bubble-type vortex breakdown. Both fire whirls and blue whirls have a typical triple-flame structure, and the position, size and shape of the triple flame vary as the liftoff distance changes. The unique flame shape of blue whirls is caused by a combination of the thermal expansion of gas and the restriction of the radial flow by the axis as the triple flame of the flame base is close to the rotating axis. The theoretical solution of the unified lifting curve of these two flame regimes under a wide range of parameters is derived and qualitatively agrees with the numerical result. The unified lifting curve contains 4 different branches, two of which are stable and the other two are unstable. The two stable branches respectively correspond to fire whirls with relatively small liftoff distances and blue whirls with greater liftoff distances. Finally, the hysteretic transition mechanism between the two flame regimes is discussed, which is expected to provide useful guidance for future experiments.

Declaration of Competing Interest

The authors declare that they have no known competing financial interests or personal relationships that could have appeared to influence the work reported in this paper.

References

[1] H. Xiao, M.J. Gollner, E.S. Oran, From fire whirls to blue whirls and combustion with reduced pollution, Proc. Natl. Acad. Sci. USA 113 (34) (2016) 9457–9462.

[2] S.B. Hariharan, E.T. Sluder, M.J. Gollner, E.S. Oran, Thermal structure of the blue whirl, Proc. Combust. Inst. (2018) 4285–4293.

[3] E. Kolb, Experimental approach to the blue whirl, UC San Diego, 2018 Ph.D. thesis.

[4] S.B. Hariharan, P.M. Anderson, H. Xiao, M.J. Gollner, E.S. Oran, The blue whirl: boundary layer effects, temperature and OH* measurements, Combust. Flame 203 (2019) 352–361.

[5] Y. Hu, S.B. Hariharan, H. Qi, M.J. Gollner, E.S. Oran, Conditions for formation of the blue whirl, Combust. Flame 205 (2019) 147–153.

[6] W. Coenen, E.J. Kolb, A.L. Sánchez, F.A. Williams, Observed dependence of characteristics of liquid-pool fires on swirl magnitude, Combust. Flame 205 (2019) 1–6.

[7] J.D. Chung, Numerical simulation of the blue whirl: A reacting vortex breakdown phenomenon, University of Maryland, College Park, 2019 Ph.D. thesis.

[8] J. Carpio, W. Coenen, A. Sánchez, E. Oran, F. Williams, Numerical description of axisymmetric blue whirls over liquid-fuel pools, Proc. Combust. Inst. (2020) 2041–2048.

[9] J.D. Chung, X. Zhang, C.R. Kaplan, E.S. Oran, The structure of the blue whirl revealed, Sci. Adv. 6 (33) (2020) eaba0827.

[10] S.B. Hariharan, Y. Hu, M.J. Gollner, E.S. Oran, Effects of circulation and buoyancy on the transition from a fire whirl to a blue whirl, Phys. Rev. Fluids 5 (10) (2020) 103201.

[11] O. Lucca-Negro, T. O'Doherty, Vortex breakdown: a review, Prog. Energy Combust. Sci. 27 (4) (2001) 431–481.

[12] S. Li, Q. Yao, C.K. Law, An analysis of the stabilization of fire whirls, Proc. Combust. Inst. 38 (3) (2021) 4587–4594.

[13] S. Li, Q. Yao, C.K. Law, The bottom boundary-layer structure of fire whirls, Proc. Combust. Inst. 37 (3) (2019) 4277–4284.

[14] S. Ghosal, L. Vervisch, Theoretical and numerical study of a symmetrical triple flame using the parabolic flame path approximation, J. Fluid Mech. 415 (2000) 227–260.